

An epidemic model for COVID-19 transmission in Argentina: Exploration of the alternating quarantine and massive testing strategies

Lautaro Vassallo^{1,2*}, Ignacio A. Perez^{1,2}, Lucila G. Alvarez-Zuzek³, Julián Amaya², Marcos F. Torres^{1,2}, Lucas D. Valdez^{1,2}, Cristian E. La Rocca^{1,2}, Lidia A. Braunstein^{1,2,4}

1 Instituto de Investigaciones Físicas de Mar del Plata (IFIMAR), CONICET -

Universidad Nacional de Mar del Plata, 7600 Mar del Plata, Buenos Aires, Argentina

2 Departamento de Física, Facultad de Ciencias Exactas y Naturales, Universidad Nacional de Mar del Plata, 7600 Mar del Plata, Buenos Aires, Argentina

3 Department of Biology, Georgetown University, Washington, D.C. 20057, United States

4 Physics Department, Boston University, Boston, Massachusetts 02215, United States

* lvassallo@mdp.edu.ar

Abstract

The COVID-19 pandemic has challenged authorities at different levels of government administration around the globe. When faced with diseases of this severity, it is useful for the authorities to have prediction tools to estimate in advance the impact on the health system as well as the human, material, and economic resources that will be necessary. In this paper, we construct an extended Susceptible-Exposed-Infected-Recovered model that incorporates the social structure of Mar del Plata, the 4^o most inhabited city in Argentina and head of the Municipality of General Pueyrredón. Moreover, we consider detailed partitions of infected individuals according to the illness severity, as well as data of local health resources, to bring predictions closer to the local reality. Tuning the corresponding epidemic parameters for COVID-19, we study an alternating quarantine strategy: a part of the population can circulate without restrictions at any time, while the rest is equally divided into two groups and goes on successive periods of normal activity and lockdown, each one with a duration of τ days. We also implement a random testing strategy with a threshold over the population. We found that $\tau = 7$ is a good choice for the quarantine strategy since it reduces the infected population and, conveniently, it suits a weekly schedule. Focusing on the health system, projecting from the situation as of September 30, we foresee a difficulty to avoid saturation of the available ICU, given the extremely low levels of mobility that would be required. In the worst case, our model estimates that four thousand deaths would occur, of which 30% could be avoided with proper medical attention. Nonetheless, we found that aggressive testing would allow an increase in the percentage of people that can circulate without restrictions, and the medical facilities to deal with the additional critical patients would be relatively low.

1 Introduction

In March 2020 the World Health Organization (WHO) officially announced the COVID-19 (disease caused by the novel SARS-CoV-2 coronavirus) as a pandemic. The world was about to witness one of the most devastating pandemics in the last decades. In December 2019, a cluster of a novel pneumonia-like illness was identified in Wuhan (China) and, without the proper control measures, in 3 months the disease rapidly spread all over the world. The first stages of the propagation occurred in different countries of Europe, leading to countless human life losses and a severe economic crisis.

On March 3, the first COVID-19 patient was confirmed in Buenos Aires, Argentina. It was an imported case, a 43-year-old man who had arrived from Milan, Italy. Following international protocols and recommendations of local experts, educational centers of all levels were closed, massive shows were suspended and international frontiers were closed. Decisively, on March 19, and in order to restrict the spread of the new coronavirus, the national government announced a 12 days nationwide lockdown [1]. These measures have been progressively extended to the present day with certain relaxations. Until the middle of September, the total number of confirmed cases surpassed 750 thousand and the number of fatalities was around 17 thousand, most of them concentrated in Capital Federal (CABA) and the suburbs, which form the urban conglomerate known as Área Metropolitana de Buenos Aires (AMBA), inhabited by 37% of the total population in Argentina.

Researchers have put a lot of effort in the study of multiple aspects of COVID-19 pandemic in several countries [2–8], at country level and at big regions with a high concentration of people [9]. Amaku *et al* [10] developed a mathematical model to study two testing strategies to halt the epidemic spread in Brazil. They found that a strategy that considers testing only infected individuals and their immediate contacts has the same effectiveness in reducing the total number of cases as a massive testing strategy but at a much lower cost. Paternina-Caicedo *et al* [11] studied an intermittent intervention strategy in Colombia that is triggered when the number of critical patients exceeds a threshold. They showed that this strategy could significantly reduce the total number of cases and prevent up to 97% of deaths from COVID-19. Cancino *et al* [12] proposed a model to study several measures to contain the epidemic spread in Chile and obtained that a combination of lockdown and contact tracing measures is the most effective strategy to reduce the peak demand for ICU beds. In the case of Argentina, Romero *et al* [13] simulated an agent-based model for COVID-19. The authors analyzed the evolution of four different pandemic scenarios, with different levels of restriction in population mobility, and they found that social isolation is the measure that has more impact in the spread of the virus. In the same way, in [14], Neidhöfer *et al* found that early school closures effectively helped in reducing the mortality rate in Argentina, Italy and South Korea. For its part, Torrente *et al* [15] showed the psychological impacts of the pandemic and the early measures implemented, in the form of substantial anxious and depressive symptoms. Moreover, Figar *et al* [16] conducted a seroprevalence study in one of the largest slums in CABA and found, three

months after the first reported case, a prevalence of 53.4%. Mobility was also analyzed in Buenos Aires City, as a proxy for effectiveness of lockdown measures. For instance, in [17], Ahumada *et al* found a delay of 8 days between changes in mobility and reported cases, while deaths follow cases from 16 to 19 days after.

Beyond the measures imposed by the government at a national level, each city in Argentina has the autonomy of taking different actions against the disease [18]. Crucial factors such as hospital capacity, demographic structure, and economic activities, among others, strongly vary between cities. Therefore, local authorities must adapt national guidelines to their own region and determine proper criteria in the decision-making process. For this reason, our study is focused in Mar del Plata (MDP), the main city of the Municipality of General Pueyrredón in Argentina. With this work we aim to provide a key study that will help local governments in decision-making and implementation of mitigation strategies, as well as estimating the medical resources required to face the consequences of such decisions.

The social and demographic structure of the population is generally reflected in heterogeneous contact patterns among individuals, where age is one of the main determinants of these mixing patterns. For instance, children tend to spend more time with children and members of their household; active adults mix with individuals in their workplace; and so forth. For this reason, a disease transmission route may have mixing patterns among individuals of different age [19]. To account for this contact structure, we use census collected data given by national agencies [20]. We divide the population into age groups and compute different contact matrices associated to different settings -household, workplace, school and general community [21, 22].

Once we obtain the Mar del Plata contact structure, we consider an extension of the compartmental Susceptible-Exposed-Infected-Recovered (SEIR) model [23] -known as SEIRD- to estimate the evolution of the epidemic. Here, D takes into account the individuals that die as a consequence of the disease. Also, we differentiate between symptomatic and asymptomatic infected individuals, considering different levels of illness severity for symptomatic patients. As in the real-life scenario, some individuals may not require medical attention at all (mild) and only will have to stay for a certain time at home, while others (severe) will require hospitalization [24].

In the context of the COVID-19 pandemic with such devastating consequences worldwide, the development and distribution of a new vaccine are crucial. However, reaching this “end game” could take too long and cost a considerable amount of deaths. For this reason, the study of non-pharmaceutical strategies to gain time is urgently needed to cease the imminent advance of the disease [25–27]. Unfortunately, measures such as long lasting quarantines also carry serious psychological and economic consequences, that must be considered. Related to this topic, Meidan *et al* [28] proposed a novel alternating quarantine strategy (AQ). In this strategy the population is separated into two groups, which alternate successively between quarantine and regular activity in a bi-weekly cycle. They found that this measure can be useful as a primary mitigation strategy, with a comparable impact to

that of a strict population-wide quarantine. Furthermore, the weekly relief allowing people an outlet to continue their activity for half of the time may, itself, increase cooperation levels. In other words, while a complete lock-down is extremely stressful for the individual, the alternating bi-weekly quarantine routine relaxes the burden, and may encourage compliance. In addition, Meidan *et al* [28] provided detailed guidelines to apply this strategy in a real scenario.

In this paper, we propose an age-stratified compartmental model for COVID-19 with an alternating quarantine strategy in which a fraction of the population can move freely at any time (q_0) while the rest is equally divided into two groups and goes through successive periods of normal activity and lockdown, each lasting τ days. We extensively explore the relationship between q_0 and τ and find that regardless of the value of q_0 , the optimal period that minimizes the total number of cases is approximately $\tau = 7$. On the other hand, an issue for low and middle-income countries is that a mass random testing strategy can be expensive to implement and would be a misuse of resources when the number of infected individuals is low. Therefore, we propose in our model a testing strategy that is triggered when the number of cases is above a threshold. We obtain that as the test rate r_0 increases, the total number of cases decreases, but this effect is diluted for high values of r_0 . Finally, we study the combination of the testing strategy and the alternating quarantine and estimate the required number of tests, as well as the demand for ICU beds. In the worst case, our model estimates that four thousand deaths would occur, throughout the entire epidemic, of which 30% could be avoided with proper intensive care. Nonetheless, if an aggressive massive testing is implemented, it would be possible to increase the percentage of people that can circulate freely, being the medical facilities required to deal with the additional critical patients relatively low. Furthermore, it is important to note that, even though we chose MDP and calibrated the model for COVID-19, our study can be adapted to any region or country where demographic information is available, and for diseases transmitted similarly by contact.

Our work is organized as follows. In section 2, we present our differential equations that govern the spread of the disease and the equations for the alternating quarantine and massive testing strategies. In section 3, we present our results for the following strategies: i) only a massive testing strategy is conducted, ii) only a quarantine strategy is applied, and iii) both strategies are applied. Finally, in section 4, we present our conclusions.

2 Model

2.1 Compartments

In this work, we use an extension of the SEIR model to study the spread of the COVID-19 in MDP. In this model individuals can be assigned to four different compartments, depending on their health status. Susceptible (S) individuals are healthy and prone to be infected, becoming exposed (E) when this occurs. At the E stage, individuals have not developed

symptoms yet and they are not contagious. With the onset of symptoms, exposed individuals become infected (I) and can propagate the disease. Finally, recovered (R) individuals have acquired immunity and no longer propagate the disease. One modification we make to this model is the addition of a compartment of deceased (D) individuals, which are usually not distinguished from the recovered individuals. Additionally, we include a compartment of undetected (U) individuals, which takes into account the infected people who do not seek medical attention because they are asymptomatic or have very mild symptoms. These individuals are able to propagate the disease (several publications [29–33] have reported the importance of asymptomatic individuals in the transmission of COVID-19).

As we are especially interested in estimating the medical resources that should be allocated to sick individuals, we model their evolution by recognizing different levels of illness severity. On the one hand, some cases develop a mild (M) version of the disease. Thus, they may not require medical care, but must remain isolated at their homes or in isolation sites prepared for this purpose, until they recover. On the other hand, some individuals develop more serious symptoms and are hospitalized (\mathcal{H}) for control. Finally, we divide the hospitalized patients into four categories, based on the fact that the evolution of each type of patient has particular characteristic times and requires different resources from the hospital:

1. H : those in general beds who will fully recover from the disease,
2. H^* : those in the intensive care units (ICU) who will fully recover from the disease,
3. H^\dagger : those in general beds who will die,
4. $H^{\dagger*}$: those in the ICU who will die.

Note that we use \mathcal{H} when referring to all compartments of hospitalized individuals together, as a set. For the different subgroups of \mathcal{H} , i.e, the H 's, we use a dagger (\dagger) as a notation to mark the compartments that evolve to the compartment D of deceased individuals, while an asterisk ($*$) denotes the compartments of individuals that make use of intensive care units (ICU).

In Fig. 1 we show a flowchart of our model. At the beginning, most of the population starts in the S compartment. With an effective rate dependent on β , susceptible individuals evolve to the E compartment, because of the interaction with the infected population. The exposed population becomes infected with rate α ; a fraction ϵ develops symptoms and progresses to the I compartment, while the remaining goes to U . We consider that symptomatic individuals do not immediately become aware of their health state, thus, we include a rate ω for the progression from I to the M and \mathcal{H} compartments. Only a fraction ζ of I individuals are hospitalized, while the remaining are isolated at home (M compartment). These isolated individuals fully recover from the disease with rate γ^m . Note that the M compartment accounts for individuals with mild symptoms who have been instructed by a healthcare professional to isolate themselves at home because they have

mild symptoms. These cases are included in the total number of COVID-19 cases reported by the authorities. On the other hand, the U compartment includes those undetected individuals: without symptoms or with mild symptoms who do not self-isolate, and can therefore spread the disease to others. On the right side of the flow chart we have the four compartments of hospitalized patients, which are differentiated by the presence of superscripts. The population going to these compartments is determined by the values of the corresponding fractions $\theta, \theta^*, \theta^\dagger$ and $\theta^{\dagger*}$, where $\theta + \theta^* + \theta^\dagger + \theta^{\dagger*} = 1$. On the other hand, the exit of these compartments is done with different γ -rates, in case the patients recover, or with different δ -rates, for fatal cases. Note that patients in the ICU who will recover, i.e., individuals in the H^* compartment, first flow to the H compartment.

The choice of multiple \mathcal{H} compartments ensures that the fractions of patients who fully recover from the disease and those who die are consistent with the values reported in the literature. These fractions are only determined by $\theta, \theta^*, \theta^\dagger$, and $\theta^{\dagger*}$, and not by the output rates (γ - and δ -rates). A summary of the states and parameters can be found in S1 Table and S2 Table.

2.2 System of equations

In an effort to better represent the society, we will divide the population into age groups and incorporate contact matrices [34, 35] to our model. These matrices indicate the mixing patterns between individuals of the population, i.e., the frequency with which people of a certain age interact with each other, and with people from different age groups. This enables us to estimate better the impact of the pandemic over the health system, and the medical resources that will be required. For the particular case of Mar del Plata, we use the census data collected by official organizations [20] and the inferring method developed in [22] to compute the matrices associated with different kinds of social settings: households, workplaces, schools, and general community. A summary of the inference method can be found in S1 Calculation.

Each age group has its own set of equations describing the evolution of the disease spread, which is indicated by the subscript i . Note that some parameters are age-dependent while others are not, indicated by the presence or absence of this subscript. The evolution of each group is given by:

$$\frac{dS_i}{dt} = -\mathcal{F}_i(t) S_i, \quad (1)$$

$$\frac{dE_i}{dt} = \mathcal{F}_i(t) S_i - \alpha E_i, \quad (2)$$

$$\frac{dI_i}{dt} = \alpha \epsilon E_i - \omega I_i, \quad (3)$$

$$\frac{dU_i}{dt} = \alpha (1 - \epsilon) E_i - \gamma^u U_i \quad (4)$$

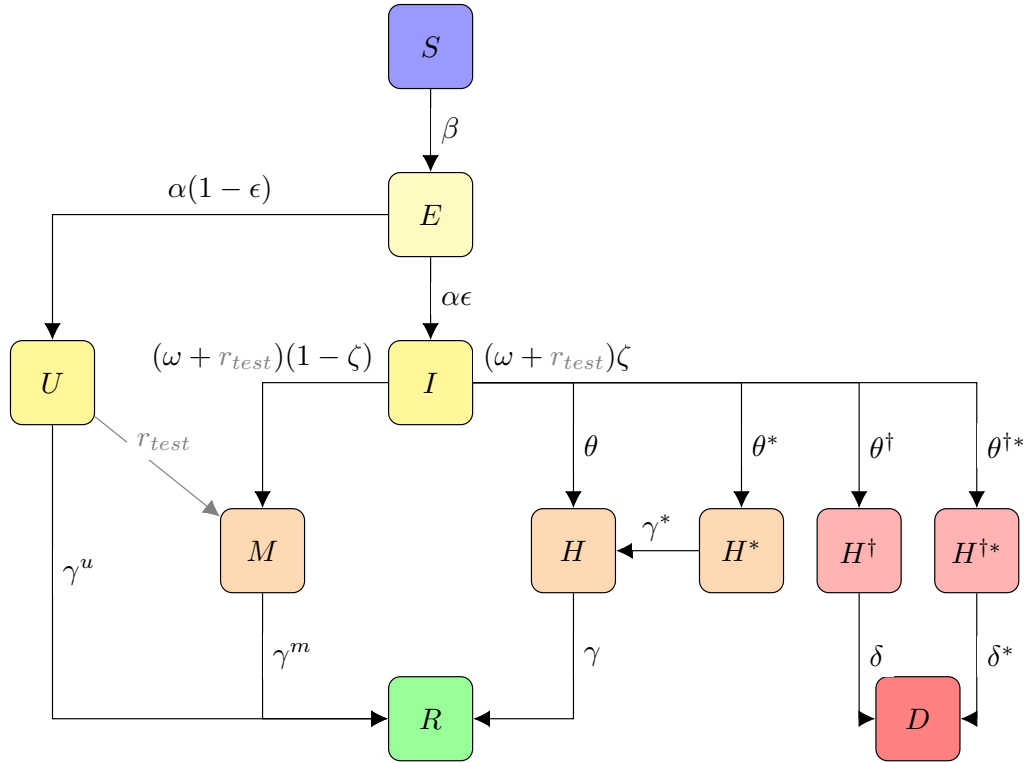


Fig 1. Flowchart of our epidemic model. The susceptible population S evolves to the exposed compartment E with an effective rate of contagion dependent on β because of the interaction with infected individuals in compartments I and U . The exposed population becomes infected with rate α ; a fraction ϵ develops notorious symptoms and progresses to the I compartment, while the remaining goes to the undetected compartment U . Symptomatic infected individuals pass to one of the compartments among the M and \mathcal{H} with a rate ω . On the right side of the flow chart we have the four hospitalized compartments, which are differentiated with the presence of superscripts. Finally, individuals can end up in one of the two final states, recovered (R) or deceased (D). Note that the gray arrow from the U to the M compartment and the term r_{test} in the outflow rates of the I compartment correspond to the testing strategy explained in subsection 2.4.

$$\frac{dM_i}{dt} = \omega (1 - \zeta_i) I_i - \gamma^m M_i, \quad (5)$$

$$\frac{dH_i}{dt} = \omega \zeta_i \theta_i I_i + \gamma^* H_i^* - \gamma H_i, \quad (6)$$

$$\frac{dH_i^*}{dt} = \omega \zeta_i \theta_i^* I_i - \gamma^* H_i^*, \quad (7)$$

$$\frac{dH_i^\dagger}{dt} = \omega \zeta_i \theta_i^\dagger I_i - \delta H_i^\dagger, \quad (8)$$

$$\frac{dH_i^{\dagger*}}{dt} = \omega \zeta_i \theta_i^{\dagger*} I_i - \delta^* H_i^{\dagger*}, \quad (9)$$

$$\frac{dR_i}{dt} = \gamma^u U_i + \gamma^m M_i + \gamma H_i, \quad (10)$$

$$\frac{dD_i}{dt} = \delta H_i^\dagger + \delta^* H_i^{\dagger*}, \quad (11)$$

where the force of infection $\mathcal{F}_i(t)$ is defined by

$$\mathcal{F}_i(t) = \sum_j C_{ij} \frac{\beta (I_j + U_j)}{N_j}, \quad (12)$$

C_{ij} is the element of the contact matrix which corresponds to the interaction strength between individuals of age groups i and j , and N_j the total number of individuals of age group j . The S1 Table and S2 Table show the parameters of our model and their values. We denote β as β_{free} for the case of free propagation without any intervention.

For our stochastic simulations, we model a population with N_j agents in each age group (see S2 Table), using a discrete time approach, where time advances in fixed Δt time steps, and the state of all agents is updated synchronously [36]. In this work, we use $\Delta t = 0.1$ days.

2.3 Alternating quarantine

In countries where the vaccine is not yet available to all citizens, it is of major importance that society implements different non-medical policies to prevent and mitigate the damages that COVID-19 may cause. Being able to estimate the amount of resources that will be needed, as the epidemic progresses, is a key aspect that authorities should seek in order to implement appropriate policies. In this section, we present a particular intervention strategy that could be helpful in accomplishing a rather controlled progression of COVID-19 in any population, although we focus in MDP, for which we use its census data.

The alternating quarantine (AQ) strategy consists in dividing the population into different groups that face alternate periods of activity/isolation in terms of their socioeconomic activities (education, work, recreation, transportation, etc.). There is one group that is permanently active (labeled as q_0). The remaining population is separated into two

equal parts (q_1 and q_2), one that is active and in contact with the q_0 group, and one that implements a strict lockdown (these isolated individuals can not propagate the disease). After an established period of time τ , q_1 and q_2 switch places. The parameter τ will be tuned in order to find the best possible scenario for diminishing the spread of the disease.

For this strategy, we subdivide each compartment S_i , E_i , I_i and U_i into three groups q_0 , q_1 , and q_2 (the labels represent also the fraction of the population in each group, so that $q_1 = q_2 = \frac{1-q_0}{2}$). Thus, adapting Eq. (12) to the case of alternating quarantine, the force of infection for each group must be rewritten as follows:

$$\mathcal{F}_i^{\mathcal{Q}}(t) = \sum_j C_{ij} \frac{\beta^{\mathcal{Q}} (I_j^{\mathcal{Q}} + I_j^{q_0} + U_j^{\mathcal{Q}} + U_j^{q_0})}{N_j}, \quad (13)$$

$$\mathcal{F}_i^{q_0}(t) = \mathcal{F}_i^{q_1}(t) + \mathcal{F}_i^{q_2}(t), \quad (14)$$

where $\mathcal{Q} = \{q_1, q_2\}$. The rates of infection are given by:

$$\beta^{q_1} = \beta_{\text{free}} \Theta \left[\sin \left(\frac{\pi t}{\tau} \right) \right], \quad (15)$$

$$\beta^{q_2} = \beta_{\text{free}} \left(1 - \Theta \left[\sin \left(\frac{\pi t}{\tau} \right) \right] \right), \quad (16)$$

where $\Theta(\cdot) \in [0, 1]$ is the Heaviside function (with $\Theta(0) = 1$), so that $\Theta \left[\sin \left(\frac{\pi t}{\tau} \right) \right]$ is a periodic square function of period 2τ . Note that β^{q_1} and β^{q_2} are perfectly out of phase.

2.4 Population-wide testing

In the context of an epidemic outbreak, identifying infected individuals is crucial to attenuate the imminent propagation as it allows authorities to isolate specific carriers of the disease [37]. Particularly, the detection of infected individuals with very mild symptoms or no symptoms at all is a difficult task to achieve, since these individuals do not know they are ill and, therefore, do not seek medical attention. It is extremely important to find and isolate them as quickly as possible. For this reason, along with the AQ strategy, we implement a random massive testing strategy with rate r_{test} in which individuals in the U compartment flows to the M compartment. Similarly, symptomatic infected individuals I will be detected by this strategy and admitted to the hospital or isolated, as previously explained. Mathematically, this means replacing in Eqs. (3), (5)-(9) ω by $\omega + r_{\text{test}}$.

A disadvantage of a massive testing strategy is that when the number of active cases in the community is low, most tests are negative and cannot be reused. Therefore, in our testing strategy, we consider that the tests are conducted only when the total number of infected individuals at time t , $I(t)$, exceeds a threshold I_0 . More specifically, we propose

the following test rate:

$$r_{test}(t) = r_0 \Theta(I(t) - I_0). \quad (17)$$

According to this strategy, if the number of infected individuals exceeds I_0 , the population is tested at a rate $r_{test} = r_0$, reducing transmission of the virus. On the other hand, when the number of infected individuals is below I_0 , the testing strategy is suspended ($r_{test} = 0$). In particular, when $I_0 \rightarrow 0$, tests are always conducted at rate r_0 , whereas in the limit $I_0 \rightarrow \infty$, tests are never conducted.

2.5 ICU capacity

In general, local and national governments make public health decisions based on the projected availability of medical resources, such as: ICU beds, general beds, ventilators, and the specialized workers needed to operate the equipment and treat the patients [38,39]. The exponential growth of COVID-19 spread may cause a quick depletion of resources and the saturation of the health system. In consequence, an important number of avoidable deaths may occur. Therefore, it is relevant to predict the evolution of ICU beds in hospitals and to foresee the consequences of their depletion. To include the impact of ICU saturation in our deterministic equations, first, we numerically solve Eqs. (7), (9), and (11) for each age group i . More specifically, we use the forward Euler method with a time step of $\Delta t = 0.1$ [days] to estimate the number of individuals in compartments H_i^* and $H_i^{\dagger*}$ at time $t + \Delta t$. Before we update the new values of H_i^* and $H_i^{\dagger*}$, we verify for each age group that the number of ICU beds will not be exceeded. If this condition is not satisfied, the excess demand for ICU beds is diverted to the D_i compartment while the computed values of H_i^* and $H_i^{\dagger*}$ at time $t + \Delta t$ are reduced, taking into account their proportional contribution to the excess demand.

In the particular case of MDP, despite the fact that the local authorities have not reported an official number of available ICU beds [40], we estimate that there are roughly 180 ICU beds in the municipality, and approximately 60 of these beds are available to accommodate COVID-19 patients [41,42].

3 Results and discussion

As mentioned in the Introduction, on March 3, 2020, Argentina’s Ministry of Health confirmed the first case of COVID-19 in the country and two weeks later a strict national lockdown was imposed, which was gradually relaxed in the following months. Although this measure was crucial to avoid an overwhelmed healthcare system and to give hospitals time to increase their capacity, it also had a negative impact on the economy. In this section, we study the scenario in which a massive testing and AQ strategies are applied on the population since September 30, 2020, dividing the analysis into four subsections.

In the first one, we estimate: i) the value of β_{free} and ii) the initial values of individuals in each compartment on September 30, 2020, by fitting the actual death curve in the city of Mar del Plata. In the second and third subsections, we analyze the AQ and massive testing strategies separately from September 30 onwards, and in the last subsection we discuss their joint effect on the epidemic spreading. Except for the first subsection, we always compute the relevant magnitudes for 300 days, i.e., until June 7, 2021, because the number of infected individuals becomes negligible after this period, for the parameter values explored in this work*.

3.1 Estimation of β_{free} and the initial conditions

In contrast to other countries where the disease spread freely for several weeks with a non-negligible number of daily cases, Argentina rapidly imposed measures two weeks after the first case was reported. Consequently, there are insufficient data to estimate the infection rate β_{free} for free propagation in Argentina, and particularly in Mar del Plata. Although the goal of our paper is not to model the beginning of the disease spreading but from September 30 onwards, the parameter β_{free} is relevant in our work since the infection force is proportional to β_{free} , for the non-quarantined individuals in the AQ strategy (see Eqs.(13)-(16)). As the basic reproduction number at the beginning of the propagation in several countries was reported to be approximately $R_0 = 2.5$ [44–46], we fit β_{free} for our model by using the next generation matrix method [47] such that the value of R_0 for Mar del Plata is also $R_0 = 2.5$ in a stage of free propagation. By doing so, we obtain that $\beta_{\text{free}} = 5.6$.

On the other hand, as of September 30, 2020, a total number of 12862 cases and 278 deaths in Mar del Plata were reported. However, due to asymptomatic cases and a low testing rate, it is to be expected that the former number was significantly underestimated. Therefore, to estimate the number of individuals in each compartment on September 30, we fit our model to the actual death curve from August 18 to September 30, obtaining $\beta = 3.45$. Note that the death curve has also been used in previous studies to estimate unknown parameters [48]. More specifically, to fit β , we integrate Eqs. (1)-(11) in this period for different values of β in the interval [2.3, 8.0]. Then we choose the optimum value that minimizes the square distance between the predicted numbers of accumulated deaths and their reported values before September 30, as shown in Fig. 2. After fitting our model, we compute the number of individuals in each compartment on that date.

Briefly, we obtained that on September 30, 2020: approximately 7,300 individuals were exposed individuals (E), 4,144 were symptomatic non-isolated individuals (I), 268 were hospitalized (53 in ICU beds), 6500 patients were isolated at home (M), and 12,000 remained undetected (U). In S3 Table, we show the estimated number of individuals in each compartment segregated by age group.

*: The code for our simulations is publicly available on Github [43].

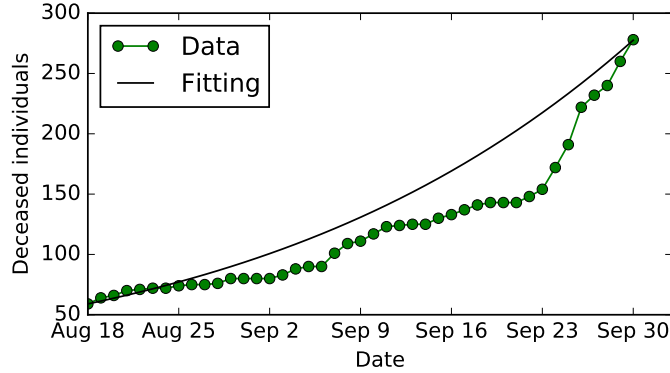


Fig 2. Fitting of the actual death curve. The solid black line represents the theoretical curve that minimizes the mean square error with the real data (green dots). The curve corresponds to $\beta = 3.45$, which allows us to estimate the initial conditions of the rest of the compartments.

3.2 Mass testing strategy without alternating quarantine

In this subsection, we will analyze the effect of a massive testing strategy on the spread of the virus without implementing the quarantine strategy, i.e., $q_0 = 1$. Figure 3A shows the time evolution of the number of infected individuals for different values of r_0 and with $I_0 = 4144$ (see Eq. (17)) which is the estimated number of infected individuals on September 30, 2020 (see Sec. 3.1). It can be seen that the strategy decreases the height of the peak, and the curve flattens around $I = I_0$. On the other hand, for the time evolution of the cumulative number of cases (Figure 3B), I_{ac} , as the value of r_0 increases, the final number of accumulated cases $I_{ac}(t = \infty)$ decreases. This result is to be expected because patients who test positive are immediately isolated, which mitigates the spread of COVID-19 in the population. However, the effect of r_0 on $I_{ac}(t = \infty)$ becomes less noticeable as r_0 increases. To explain this behavior, in S2 Calculation, using a SIR model with a testing rate given by Eq. (17), we study in detail the limit $r_0 = \infty$. In particular, we show in S2 Calculation that as r_0 increases in Eq. (17), the curves of infected individuals $I(t)$ approach the case of $r_0 = \infty$, in which $I(t)$ remains constant at $I = I_0$ for a period of time, as a consequence of the activation-deactivation of the strategy around this value. During this plateau, the number of susceptible individuals decreases until the population reaches herd immunity, and from this moment on, the number of infected individuals declines exponentially. Therefore, a testing strategy with a test rate given by Eq. (17) is effective in flattening the curve of infections and avoiding an overwhelmed healthcare system. However, if it is not combined with other measures to lower the probability of infection, then a large number of individuals will have been infected by the end of the epidemic.

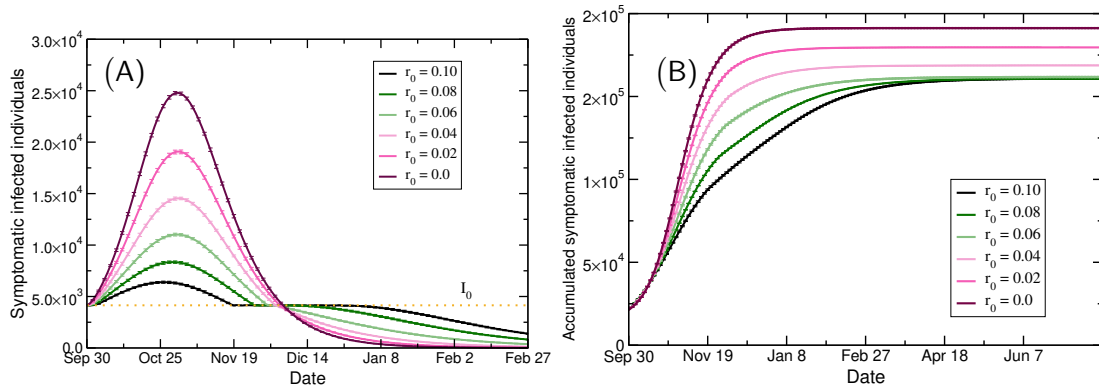


Fig 3. Mass testing effect on infected population. (A) The number of symptomatic infected individuals (I) and (B) the accumulated number of symptomatic infected individuals (I_{ac}) predicted by our model for different values of the testing parameter r_0 and $q_0 = 1$ (no quarantine) and $I_0 = 4144$. The error bars were estimated from 50 stochastic simulations.

In the supplementary material, S4 Table and S5 Table, we show the impact of different thresholds I_0 on the total number cases and tests used until June 7, 2021. Since in Mar del Plata the epidemic was under control on September 30 when the number of infected individuals was 4144, in the following sections we explore the impact of testing strategy on the epidemic only for $I_0 = 4144$.

3.3 Alternating quarantine without mass testing

Now we study the effect of the AQ on the epidemic spreading for different values of τ and q_0 , without implementing the testing strategy ($r_{test}(t) = 0$). To this end, we solve numerically Eqs. (1)-(11) and compute the cumulative number of infected individuals at the final state (when $I \approx 0$), and the height of the peak of active cases under the AQ routine. In Fig. 4, these two quantities are plotted as a function of the period τ , which ranges from 1 to 14 days. To easily compare the curves of different values of q_0 , we applied a min-max normalization [49] to show the y-coordinates in the interval $[0, 1]$. As can be seen, the optimal value of τ is weakly dependent of the parameter q_0 , with approximately 8 days being the optimum for the accumulated cases (Fig. 4A) and between 7 and 8 days for the peak of active cases (Fig. 4B). From here on, we use $\tau = 7$ in our simulations as it is close to optimal, and in this way, the AQ can be in phase with the standard week.

3.4 Joint effect of the testing and AQ strategies

In this last subsection, we will study the joint effect of the testing and AQ strategies on the epidemic spreading and how they reduce the pressure on the health system. In Fig. 5A, we show a heat map of the peak value of symptomatic infected individuals (I) as a

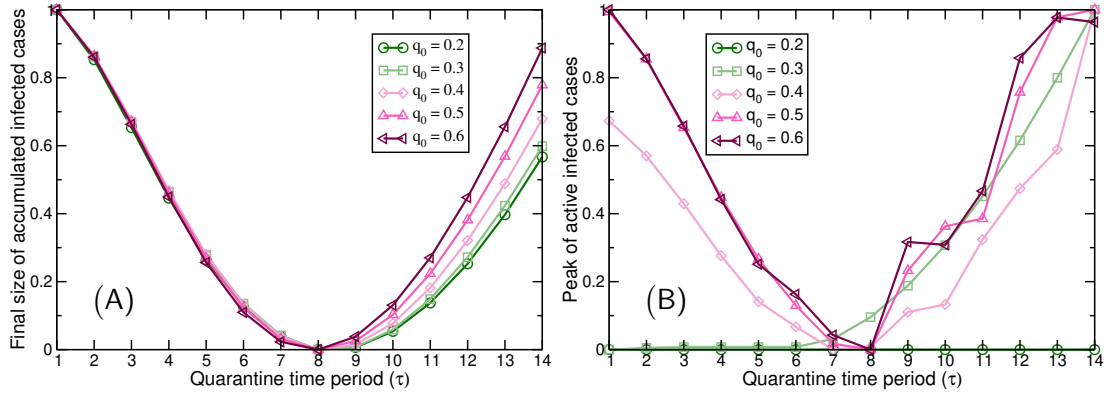


Fig 4. Optimal value of τ . (A) The accumulated number of infected individuals at the final state and (B) the height of the peak of active cases as a function of τ for different values of the parameter q_0 . The values were obtained by solving numerically Eqs. (1)-(11).

function of the fraction of the permanently active population q_0 and the test rate r_0 , for $I_0 = 4144$ (see Eq. (17) and Sec. 3.2). It can be seen that there is a region where the peak coincides with the initial value of infected individuals, implying that the curve of infected cases can no longer grow after applying both strategies. In contrast, for higher values of q_0 and lower values of r_0 , the peak of infected individuals is up to 6 times higher than the threshold I_0 . On the other hand, in Fig. 5B, the final sizes of accumulated symptomatic infected individuals on June 7, 2021, are shown. As in the first sub-figure, the AQ strategy reduces significantly this magnitude when the value of q_0 decreases. It can also be noted from the vertical iso-height lines, that high values of r_0 cannot reduce the final size of the epidemic, which is consistent to the results shown in Section 3.2. Note that the magnitudes shown in Figs 5A-B, correspond only to detected individuals, i.e., the cases that passed through compartments M and \mathcal{H} , but if we also include the individuals who passed through compartment U , we obtain qualitatively similar results. In the supplementary material we present additional results for the number of infected individuals compared with the real data after September 30 (see Fig. S1).

To further elucidate the impact of the epidemic spreading on the health system, we will compute the minimum number of ICU beds (B_{min}) to prevent an overwhelmed healthcare system. In order to estimate this magnitude we compute the time evolution of the number of critical patients when there is no restriction on the number of ICU beds, as shown in Fig. 6A, for an increasing value of r_0 and $q_0 = 0.7$. Note that the height of the peak of this curve indicates the value of B_{min} that prevents ICU saturation. In Fig. 6B we plot a heat map of B_{min} and we obtain, as expected, that the two proposed strategies reduce the pressure on the health system, i.e., B_{min} decreases for larger values of r_0 and smaller values of q_0 . Note that the region to the left side of each isoline of B_{min} (solid black lines) corresponds

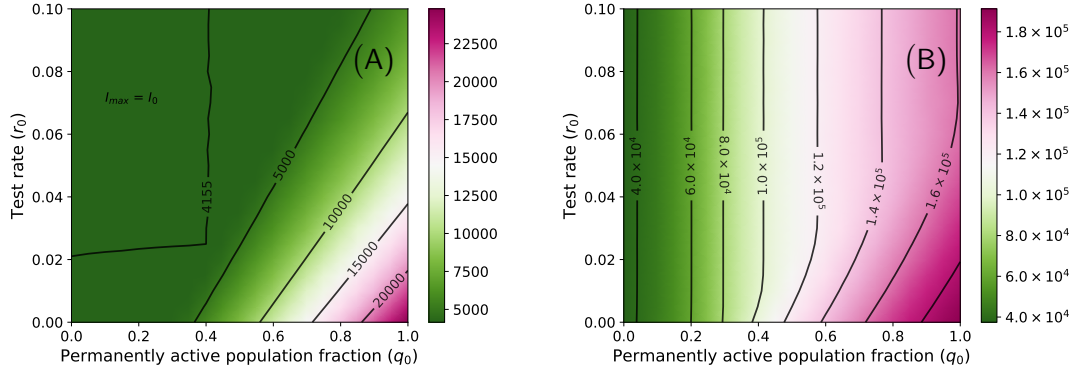


Fig 5. Evolution of infected individuals. In (A) we show a heat map of the height of the peak of symptomatic infected individuals I_{max} in the plane q_0 - r_0 . The black lines represent isolines. In panel (B), in a similar way, the final sizes of accumulated symptomatic infected individuals are shown, after 300 days of simulation.

to the values of q_0 and r_0 where the demand for ICU resources does not exceed the supply B_{min} . In the supplementary material (see Fig. S2), we include a heat map of the period of time in which the health system is overwhelmed when the number of ICU beds is 60.

In addition, it is also relevant to estimate the total number of tests T_{test} that the municipality must purchase for a given value of r_0 and q_0 because this magnitude can be used to assess the budgetary impact of a massive testing strategy. To estimate this magnitude, we accumulate from our equations, the number of tests used per unit time for 300 days since September 30. The results of this procedure are shown in Fig. 6B as T_{test} -isolines in the plane q_0 - r_0 (dashed blue lines). The intersection between the left region of a T_{test} -isoline and a B_{min} -isoline indicates the values of q_0 and r_0 that meet the budget and ICU capacity. Notably, for a given value of q_0 , the total number of tests saturates as the testing rate r_0 increases, which is observed in the figure as a vertical T_0 -isoline.

On the other hand, since the ICU bed capacity is a critical bottleneck for the health care system, policymakers must know the total number of deaths D_{tot} if the ICU capacity is not increased, and also how many deaths would be avoided if the hospitals ensured a minimum number of ICU beds to prevent saturation. In Fig. 6C we show a heat map of D_{tot} at the final state when the number of ICU beds is 60. In the range of explored values, we observe that decreasing the fraction of permanently active individuals (q_0) reduces D_{tot} more significantly than a higher testing rate r_0 . Furthermore, the massive testing strategy has a meaningful effect on D_{tot} only when $q_0 \gtrsim 0.7$. We also include in the same figure the isolines of the number of deaths avoided (dashed blue lines) in the scenario where the authorities extend the ICU capacity to prevent an overwhelmed health care system. It can be seen that for the case of a weak AQ strategy (high values of q_0) the total number of

deaths due to the lack of ICU beds ranges from 250 to 1000 people which corresponds to up to 30% of the total number of deaths.

4 Conclusion

In this paper, we studied a combination of mitigation strategies to prevent the spread of the SARS-CoV-2 without a total restriction of activities and we applied our model to the particular case of the city of Mar del Plata. This model is based on an extended SEIR model, where detected cases are confined and do not propagate the disease. One of the strategies consists of an alternating quarantine where a portion of the population remains always active, while the rest is divided in two groups and enters a cycle of activity and isolation with period 2τ . We found that a time-window of $\tau = 7$ days is the best alternative as it reduces the peak of active cases and the final size of cumulative cases of detected symptomatic patients (a fraction of which eventually die), while it fits with the usual weekly cycle, being easy to implement. However, it should be noted that this optimal value of τ depends on the characteristic times associated with the infectious process of COVID-19, so it should be readjusted if this quarantine strategy is to be applied to mitigate other diseases. On the other hand, we studied a testing strategy on the general population with a threshold. We focused on the pressure applied to the health system and the death toll that an overwhelmed system may cause. We found that, given the situation in Mar del Plata as of September 30, extremely low levels of normal circulation would be necessary in order to avoid the saturation of the health system, regardless of the testing rate. The number of ICU beds necessary to prevent saturation increases with the fraction of the population that remains always active, but this number can be shortened by means of an aggressive testing strategy. In the worst case scenario, we estimate that thousands of people may die, but would not if properly assisted. Therefore, we consider that implementing an alternating quarantine strategy with high testing rates and medium-to-low levels of free circulation is fundamental in order to change the trend of COVID-19 spread in Mar del Plata. Authorities might have to balance testing and equipment costs with mobility levels of the population, in order to arrive at a consistent strategy that people are able to follow, thus, ensuring compliance and reducing the economic, social and psychological effects that long and extended - or the lack of - quarantine produces.

Finally, we remark that the results shown in this work should be taken with caution because our model does not consider: viral mutations, additional measures (such as the extended use of face masks or contact tracing), imported cases, seasonality effects, or a dynamic value of q_0 due to quarantine fatigue. However, we believe that our model could serve as a support for future work on the effectiveness of an alternating quarantine and massive testing strategies in more realistic scenarios.

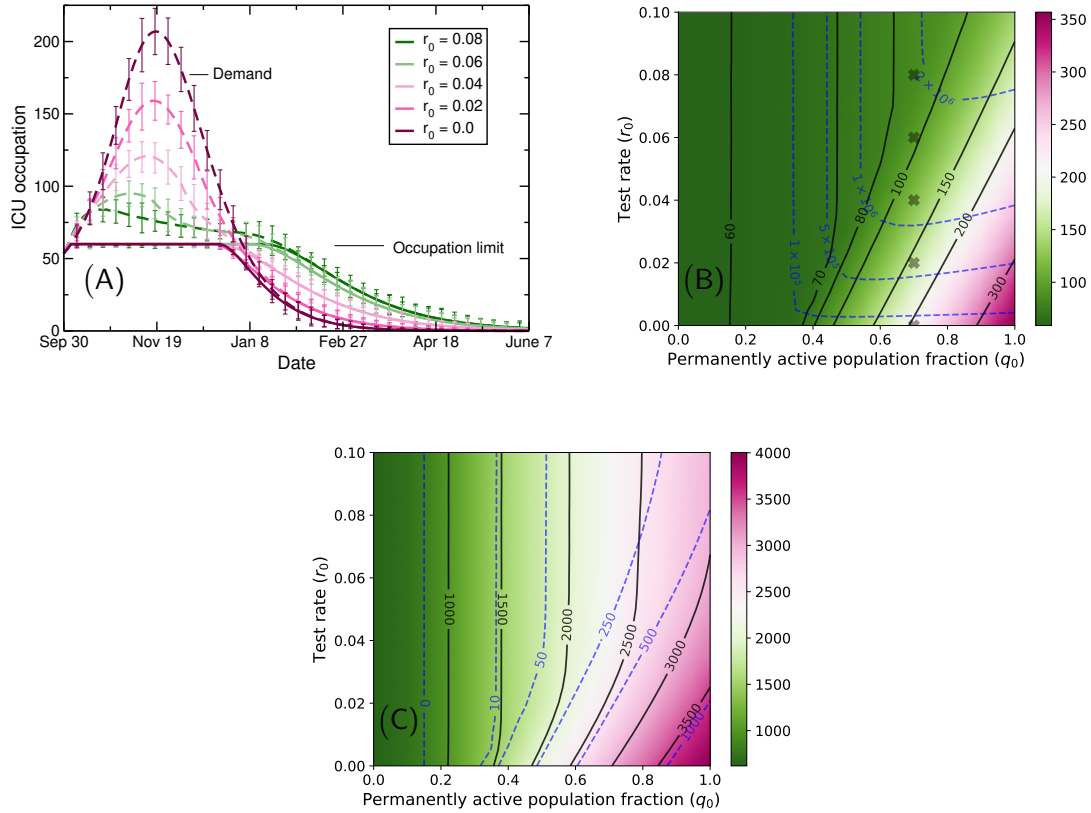


Fig 6. Impact on the health system. (A) Time evolution of the ICU occupation when the number of ICU beds is 60 (solid lines) and infinite (dashed lines). Each curve corresponds to a different value of the test rate r_0 , with $q_0 = 0.7$ and $I_0 = 4700$. The error bars were estimated from 40 stochastic simulations. (B) Heat map showing the minimum number of ICU beds (B_{min}) to prevent hospital saturation in the plane q_0 - r_0 . The black lines represent isolines while the cross marks serve as a reference for panel (A). The dashed blue lines correspond to the T_{test} -isolines (see explanation in the main text). (C) Heat map depicting the total number of deceased individuals (D_{tot}) at the final state of the epidemic in the plane q_0 - r_0 when the total number of ICU beds is 60. The solid black isolines correspond to the total number of deaths (D_{tot}) while the dashed blue isolines represent only those deaths due to hospital saturation.

Supporting material

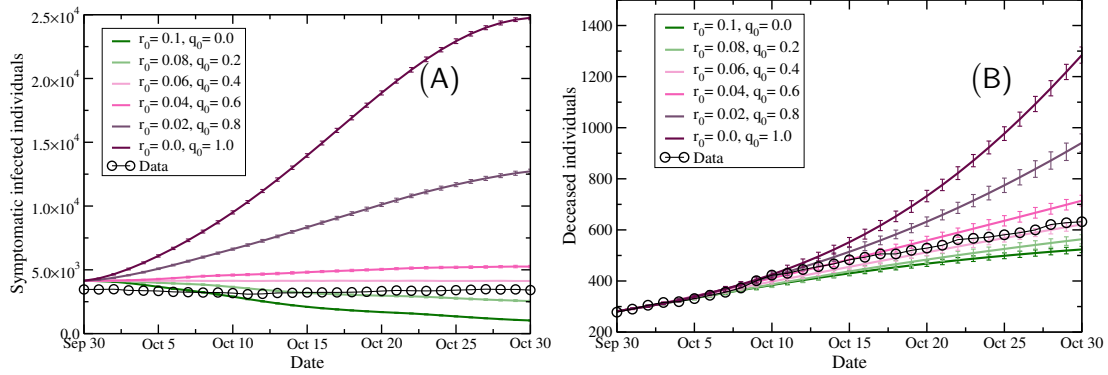


Fig S1. Comparison with real data. Predictions of our model for the number of infected individuals (panel A) and deaths (panel B) from September 30, 2020 to October 30, 2020, for some values of r_0 and q_0 (in solid colored lines) *. In both panels, we also show the actual time series (symbols). The error bars were estimated from 50 stochastic simulations. From these curves, we observe that in a scenario where $q_0 \approx 0.4$ (i.e., 40% of the population is permanently active) and $r_0 \approx 0.06$, the strategies lead to a number of cases and deaths similar to those observed in the real data. However, unlike the real case in October (according to Google’s mobility data [50]), where the mobility was 40% and 50% below baseline at workplaces and retail establishments, respectively, under this strategy, $40\% + 30\% = 70\%$ of the population would be active every week, which may benefit the local economy.

*: We excluded the data point for October 1, 2020, because health authorities in MDP reported a sharp increase in deaths caused by delayed reporting.

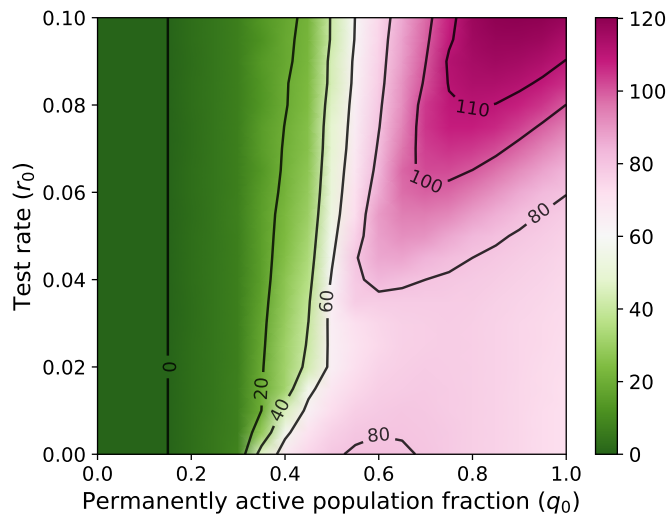


Fig S2. Number of days with an overwhelmed health system. Heat map of the number of days in which hospitals are overwhelmed in the plane $r_0 - q_0$ when the number of ICU beds is 60. In the upper right region, this period increases because a higher testing rate delays the extinction of the disease by several weeks, and a weak alternating quarantine ($q_0 \approx 1$) leaves a large proportion of the population exposed to COVID-19.

S1 Calculation. Inference of contact matrices. To compute the matrix of an arbitrary setting Δ (e.g., workplaces), we assume a homogeneous mixing for the contacts occurring at a given location U (e.g., a particular school, company, or household). We denote $a_j^{(k)}$ as the number of individuals of age j interacting with an individual k at a given place U and denote $v_\Delta^{(k)}$ as the total number of individuals of all ages within this location. Following [22], the frequency of contacts between individuals of age groups i and j , in all settings of type Δ , is given by

$$f_{ij}^\Delta = \begin{cases} \frac{1}{n_i^\Delta} \sum_{k=1}^{N_i} \frac{a_j^{(k)} - \delta_{ij}}{v_\Delta^{(k)} - 1} & \text{if } v_\Delta^k > 1, n_i^\Delta > 0 \\ 0 & \text{otherwise} \end{cases},$$

where N_i is the total number of individuals of age group i in the entire population, and n_i^Δ is the number of individuals of age group i with nonzero contacts in the setting Δ . Note that the Kronecker delta (δ_{ij}) in the numerator avoids counting k as a self-contact and the factor n_i^Δ is necessary to normalize its rows, i.e., $\sum_i f_{ij}^\Delta = 1$. After computing f_{ij}^Δ , the contact matrix associated with setting Δ is given by

$$C_{ij}^\Delta = \frac{n_i^\Delta}{N_i} f_{ij}^\Delta, \quad (18)$$

where we multiply the frequency of contacts by the probability of having at least one contact in that setting. Performing this calculation for households, workplaces, schools and the general community, we obtain a final expression for the contact matrix by taking the weighted sum

$$C_{ij} = \sum_{\Delta} \omega^\Delta \frac{C_{ij}^\Delta}{\sum_i \sum_j C_{ij}^\Delta}, \quad (19)$$

where the weight ω^Δ represents the proportion of transmission events that take place in setting Δ . Note that the matrices for each setting are divided by a normalization factor $\sum_i \sum_j C_{ij}^\Delta$.

Fig. S3 includes a graphic representation of the normalized matrices $\frac{C_{ij}^\Delta}{\sum_i \sum_j C_{ij}^\Delta}$ that were calculated for the four different settings*. It can be seen that the school and work matrices concentrate contacts in specific regions, while the home matrix is more dispersed. Regarding the contact matrix within workplaces, the low values on the diagonal are due to lack of sufficient data to compute this matrix. On the other hand, the community contact matrix represents contacts that are totally random, so that the frequency of contacts with a certain

*: We have made the contact matrices publicly available on GitHub [43].

age group is proportional to the population in this group.

In [22], the authors estimate the following weights based on empirical data for influenza-like diseases:

$$w^{house} = 0.30,$$

$$w^{work} = 0.19,$$

$$w^{school} = 0.18,$$

$$w^{comm} = 0.33.$$

We use these weight's values in Eq. (19) to fit β_{free} (see Sec. 3.1) and for the non-quarantined population in the AQ strategy (see Fig. S4A). According to Google mobility reports as of August 14 (average of 7 days), activity in workplaces was decreased by 31%, and in transit stations and retail & recreation by 75% (average between both settings). Added to the fact that all schools were closed, we used these percentages to decrease the previous weight factors, which we used to fit the curve of accumulated deaths in General Pueyrredón from August 18 to September 30 (prior to implementing the mitigation strategies in our simulations):

$$w^{house} = 0.79,$$

$$w^{work} = 0.13,$$

$$w^{school} = 0.0,$$

$$w^{comm} = 0.08.$$

In this way, we estimate the number of individuals in each compartment segregated by age group, on September 30, 2020 (see Sec. 3.1 and Fig. S4B).

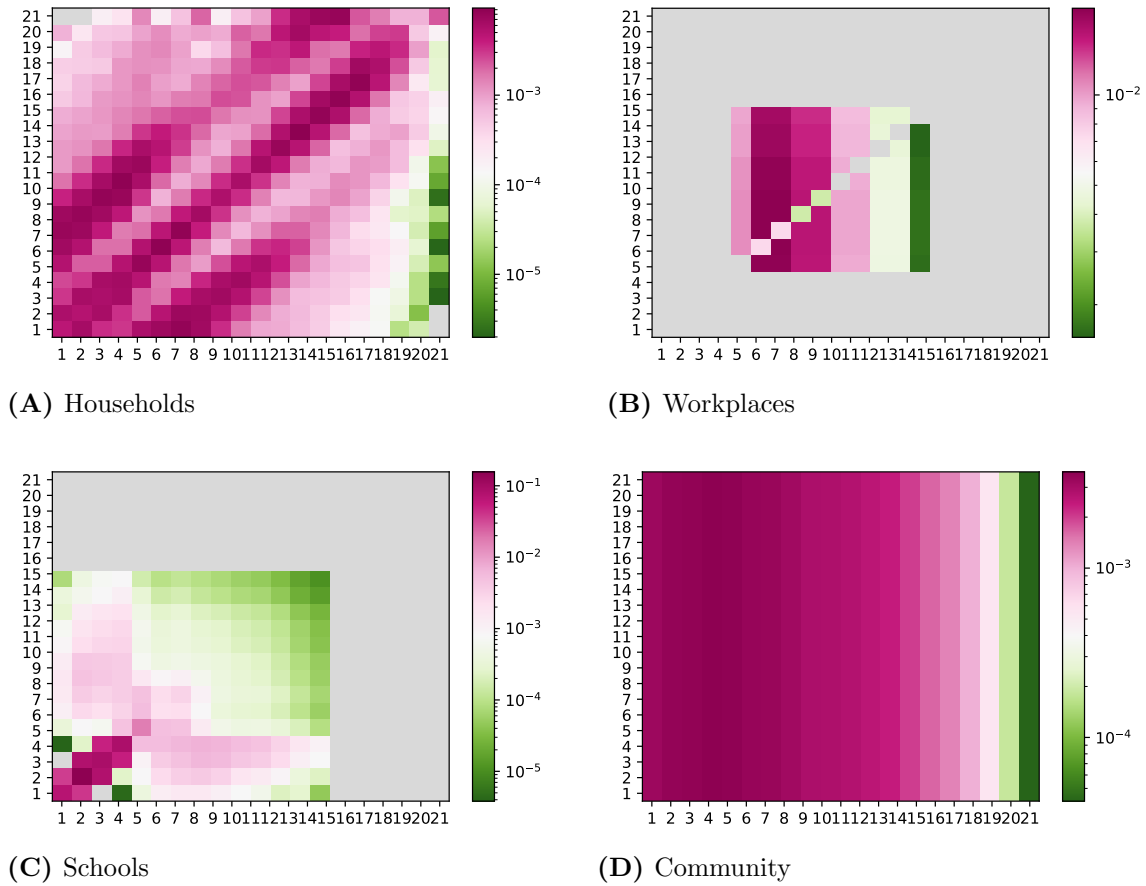


Fig S3. Contact matrices. Heat map in logarithmic scale for the contact matrix of the different social settings (see Eq. (18)). The axes indicate the 21 age cohorts considered in our model, each covering an age range of 5 years. For example, the first cohort covers from 0 to 4 years old, the second one from 5 to 9 years old, and so on. The gray color corresponds to $C_{ij}^{\Delta} = 0$.

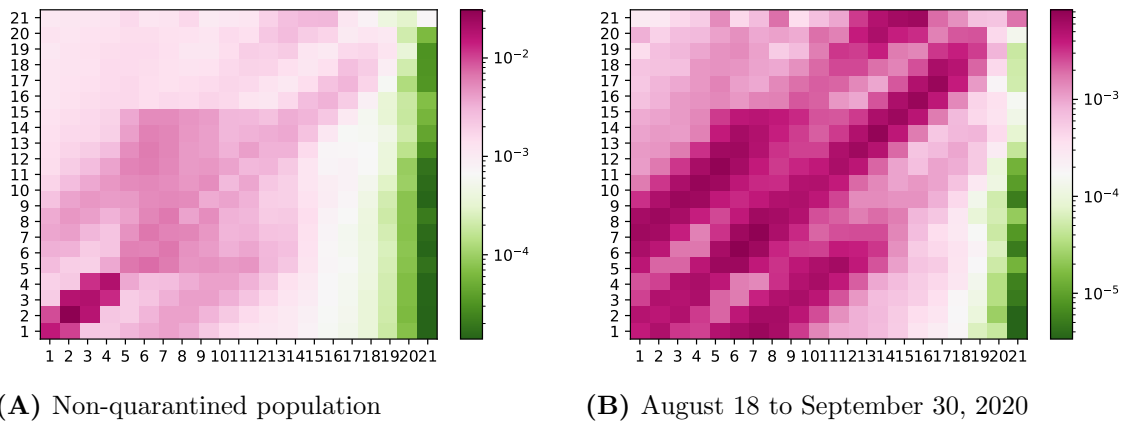


Fig S4. Total contact matrices. Heat map in logarithmic scale for the contact matrix given by Eq. (19) for: non-quarantined individuals in the AQ strategy (panel A) and for the period August 18 to September 30, 2020 (panel B).

S2 Calculation. Simplified analysis of the effect of a threshold in the testing strategy on the accumulated number of infected cases. In Sec. 2.4 we included in our model a testing rate that obeys the following function:

$$r_{test}(t) = r_0 \Theta(I(t) - I_0), \quad (20)$$

where I_0 is a threshold for the number of infected individuals, above which random testing is conducted with a rate $r_{test} = r_0$, whereas below I_0 , the testing strategy is suspended ($r_{test} = 0$). In Fig. 3B it was observed that the strategy cannot contain the number of accumulated cases I_{ac} from the start of the epidemic, even for large values of r_0 . This is because the testing strategy is suspended when $I < I_0$, regardless of the value of r_0 . To determine analytically the final number of accumulated cases for $r_0 \rightarrow \infty$, in this section we present a susceptible-infected-removed model without age structure, where individuals are tested at a rate r_{test} given by Eq. (20). For this model, the dynamic equations are as follows:

$$\frac{dS}{dt} = -\beta \frac{S}{N} I, \quad (21)$$

$$\frac{dI}{dt} = \beta \frac{S}{N} I - (\gamma + r_{test}(t)) I, \quad (22)$$

$$\frac{dR}{dt} = (\gamma + r_{test}(t)) I, \quad (23)$$

where:

1. S , I , and $R = N - S - I$ are the number of susceptible, infected, and removed individuals, respectively, and N denotes the size of the population. Here an individual is removed if he/she recovers or tests positive.
2. β is the infection rate.
3. γ is the recovery rate.

When the strategy is applied, i.e. $I > I_0$, the effective reproduction number at time t [51] is

$$R_t^{on} = \frac{\beta}{(\gamma + r_0)N} S(t), \quad (24)$$

where the superscript "on" indicates that the strategy is implemented. Analogously, when $I < I_0$, the effective reproduction number is

$$R_t^{off} = \frac{\beta}{\gamma N} S(t). \quad (25)$$

Note that $R_t^{off} \geq R_t^{on}$. In Fig. S5A) we show the time evolution of the fraction of removed individuals, where it is observed (as in Fig. 3B) that the effect of an increasing value

of r_0 on $R(t \rightarrow \infty)$ becomes negligible. On the other hand, in Fig. S5B) we show the time evolution of active cases. After this magnitude reaches the threshold of I_0/N , $I(t)/N$ oscillates around I_0/N for a period of time because the testing strategy is applied and suspended intermittently when $I(t)$ is greater and less than I_0 , respectively. In addition, we observed that the oscillation amplitude is small compared with I_0 (see inset of Fig. S5B), so the infection curve flattens or becomes approximately a plateau. However, during this period, the number of susceptible individuals is still decreasing (see Fig. S5C), and the curve $I(t)$ remains approximately flattened until the number of susceptible individuals reaches a value such that $R_t^{off} = 1$, that is, the number of cases cannot increase even when the strategy is suspended. From this moment, that we call $t = t^*$, the population has achieved herd immunity. Using that $r_0 \gg 1$ and $I(t^*) \approx I_0$, the size of the susceptible population at time $t = t^*$, denoted as S^* , is given by the condition $R_t^{off} = 1$, i.e.,

$$R_{t^*}^{off} = 1 \Rightarrow \frac{\beta}{\gamma N} S^* = 1 \Rightarrow S^* = \frac{\gamma N}{\beta}. \quad (26)$$

Then, for $t \geq t^*$, the number of infected individuals remains below I_0 , and Eqs. (21)-(23) are reduced to an SIR model without testing intervention, which is described by the following set of equations:

$$\frac{dS}{dt} = -\beta \frac{S}{N} I, \quad (27)$$

$$\frac{dI}{dt} = \beta \frac{S}{N} I - \gamma I, \quad (28)$$

$$\frac{dR}{dt} = \gamma I, \quad (29)$$

If we assume that $r_0 \gg 1$, the initial condition for these equations at $t = t^*$, are given by: $S(t^*) = S^*$, $I(t^*) = I_0$, and $R(t^*) = N - S(t^*) - I(t^*)$, and the solution of Eqs. (27)-(29) satisfies the following equation:

$$S(t^*) + I(t^*) - \frac{\gamma N}{\beta} \ln(S(t^*)) = S(t) + I(t) - \frac{\gamma N}{\beta} \ln(S(t)), \quad (30)$$

for $t > t^*$. Finally, at infinite time, as $I(t) \rightarrow 0$, and $S(t \rightarrow \infty) = N - R(t \rightarrow \infty)$, the Eq. (30) is reduced to:

$$S(t^*) + I(t^*) - \frac{\gamma N}{\beta} \ln(S(t^*)) = (N - R(t \rightarrow \infty)) - \frac{\gamma N}{\beta} \ln(N - R(t \rightarrow \infty)), \quad (31)$$

and using that the number of accumulated cases I_{ac} is equal to the number of removed individuals R , in the limit $t \rightarrow \infty$, and replacing Eq. (26) and $I(t^*) = I_0$ in Eq. (31), we

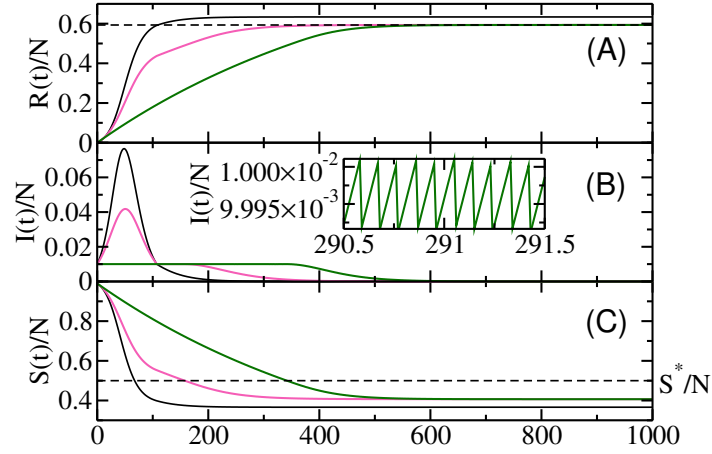


Fig S5. Simplified model results. Time evolution of the fraction of accumulated cases (panel A), active cases (panel B), and susceptible individuals (panel C) obtained from Eqs. (21)-(23) with $\beta = 0.2$, $\gamma = 0.1$, $I_0 = 0.01$, and different values of r_0 : 0.03 (solid black), 0.05 (solid pink), and 0.10 (solid green). Here, we also use as initial condition $I(t = 0) = I_0$, and $S(t = 0) = N - I_0$. In panel (A), the dashed line indicates the final number of accumulated cases for $r_0 \gg 1$, predicted by Eq. (32). In panel (B) the inset shows an enlargement of the main figure. In panel (C), the dashed line indicates the value of S^* , obtained from Eq. (26).

finally obtain that $I_{ac}(t \rightarrow \infty)$ for $r_0 \gg 1$ satisfies the equation:

$$\frac{\gamma N}{\beta} + I_0 - \frac{\gamma N}{\beta} \ln\left(\frac{\gamma N}{\beta}\right) = (N - I_{ac}(t \rightarrow \infty)) - \frac{\gamma N}{\beta} \ln(N - I_{ac}(t \rightarrow \infty)). \quad (32)$$

The solution of $I_{ac}(t \rightarrow \infty)$ is shown as a dashed line in Fig. S5A), which agrees to the limit number of accumulated cases in the final state as r_0 increases. Therefore, as mentioned in Sec. 3.2, a testing strategy with a test rate given by Eq. (20) is effective in flattening the curve of infections but cannot completely contain the disease spread from the start of the epidemic.

S1 Table. Age-independent parameters. Table describing the age-independent parameters and their values.

Symbol	Description	Value [<i>days</i> ⁻¹]	Reference	Notes
β_{free}	rate $S \rightarrow I$	5.6	[44–46]	†
α	rate $E \rightarrow I$	1/(5.1-2.0)	[45, 52–54]	‡
ω	rate $I \rightarrow M, \mathcal{H}$	1/(4.0+2.0)	[54, 55]	‡
γ	rate $H \rightarrow R$	1/8	[19]	
γ^*	rate $H^* \rightarrow H$	1/10	[19]	
γ^m	rate $M \rightarrow R$	1/14	[56]	⊘
γ^u	rate $U \rightarrow R$	1/9.5	[57]	
δ	rate $H^\dagger \rightarrow D$	1/8	[55]	
δ^*	rate $H^{\dagger*} \rightarrow D$	1/11	[55]	

†: These works report the value of R_0 in the stage of free propagation, from which we calculate β_{free} using the next generation matrix method [47].

‡: We subtract two days from the time of transition $E \rightarrow I$ reported in [45, 52, 53], since in [54] the authors estimated that patients are infectious two days before showing symptoms. Therefore, infectious patients also stay two additional days in the community, increasing the time of transition $I \rightarrow M$ and $I \rightarrow \mathcal{H}$ reported in [55].

⊘: Health authorities in Argentina require mild patients to remain self-isolated at home, and these cases are reported as recovered after 14 days since their first symptoms appeared.

S2 Table. Age-dependent parameters. Table describing the age-dependent parameters and their values. The age groups are 5 years wide.

Symbol	Description	Values for Ages [0-4, 5-9, ..., 100-104]	Ref.
N_j	Number of individuals in age group j	44797, 47945, 48457, 51013, 50015, 47266, 46560, 43238, 39557, 39067, 37358, 34966, 32699, 27311, 22564, 18999, 13780, 7680, 2532, 582, 58	[20]
ϵ	Proportion of infected individuals that will develop symptoms	1/3, 1/3, 1/3, ..., 1/3, 1, 1, 1	[16, 58] [†]
ζ	Proportion of cases that need hospitalization (\mathcal{H})	0.07504484, 0.03803735, 0.02837104, 0.0211873, 0.01936113, 0.02174475, 0.02556259, 0.02665036, 0.03077249, 0.03761504, 0.04842162, 0.0635869, 0.09234972, 0.12900137, 0.17795732, 0.22363486, 0.2618449, 0.28956643, 0.29179373, 0.28364116, 0.1965602	[55] [‡]
θ	Proportion of hospitalized patients in general beds who will fully recover	0.93138011, 0.94563427, 0.96491228, 0.9447619, 0.95835351, 0.95063985, 0.94168139, 0.91165612, 0.86417323, 0.81459711, 0.73918075, 0.65684799, 0.53099676, 0.42928786, 0.37042989, 0.31017208, 0.29837518, 0.25360883, 0.25273159, 0.25426357, 0.1625	[55] [‡]
θ^*	Proportion of hospitalized patients in ICUs who will fully recover	0.04240555, 0.04448105, 0.02232855, 0.03047619, 0.01985472, 0.019805, 0.02726584, 0.03718354, 0.05068898, 0.05412687, 0.06202268, 0.07073748, 0.06057536, 0.05436309, 0.04901567, 0.03942496, 0.03126539, 0.02462496, 0.02185273, 0.01705426, 0.0	[55] [‡]
θ^\dagger	Proportion of hospitalized patients in general beds who will die	0.00693909, 0.00329489, 0.00637959, 0.01142857, 0.00920097, 0.01279707, 0.01514769, 0.02109705, 0.03617126, 0.05167769, 0.08585975, 0.11180391, 0.18314425, 0.26018054, 0.34491764, 0.42191244, 0.48375185, 0.55165582, 0.59619952, 0.62325581, 0.65	[55] [‡]
$\theta^{\dagger*}$	Proportion of hospitalized patients in ICUs who will die	0.01927525, 0.00658979, 0.00637959, 0.01333333, 0.0125908, 0.01675807, 0.01590507, 0.03006329, 0.04896654, 0.07959833, 0.11293682, 0.16061062, 0.22528363, 0.25616851, 0.2356368, 0.22849052, 0.18660758, 0.17011039, 0.12921615, 0.10542636, 0.1875	[55] [‡]

[†]: This value was obtained from a seroprevalence study in the city of Buenos Aires, Argentina [16, 58].

[‡]: [55] is a detailed dataset of all officially reported COVID-19 cases in Argentine health institutions, including the type of treatment and its outcome.

S3 Table. Estimation of initial values. This table shows the estimated population in the different compartments by age groups as of September 30, 2020, which are used as initial conditions for the AQ and massive testing strategies.

Compartment	Values for Ages [0-4, 5-9, ..., 100-104]	Total
<i>S</i>	39469.7, 42322.4, 42827.7, 45090.7, 42681.2, 40441.2, 39943.5, 37147.8, 34024.8, 33640.0, 32117.3, 30080.9, 28367.3, 23923.8, 20704.4, 17545.8, 12763.4, 7129.8, 2332.7, 537.9, 52.5	573144.6
<i>E</i>	472.0, 498.9, 500.0, 525.8, 640.6, 596.8, 579.7, 534.5, 485.9, 476.5, 459.4, 428.2, 381.2, 299.9, 168.7, 132.4, 92.67, 50.13, 18.12, 4.034, 0.5280	7346.0
<i>U</i>	771.8, 815.3, 816.7, 859.0, 1054.1, 981.5, 952.6, 877.7, 797.6, 782.3, 754.7, 703.5, 625.2, 490.6, 273.1, 213.9, 149.7, 80.99, 0.000, 0.000, 0.000	12000.2
<i>I</i>	264.3, 279.2, 279.7, 294.2, 360.3, 335.6, 325.7, 300.2, 272.8, 267.6, 258.1, 240.6, 213.9, 167.9, 93.76, 73.48, 51.41, 27.82, 30.21, 6.720, 0.8818	4144.3
<i>M</i>	406.0, 445.8, 451.0, 477.9, 590.8, 548.6, 530.0, 487.5, 441.0, 429.6, 410.0, 376.1, 323.5, 243.1, 126.6, 93.53, 62.22, 32.41, 35.16, 7.900, 1.168	6519.9
<i>H</i>	20.84, 11.34, 8.488, 6.573, 7.439, 7.716, 8.770, 8.225, 8.289, 9.423, 10.76, 11.90, 12.46, 11.13, 7.358, 6.036, 4.683, 2.370, 2.568, 0.5504, 0.03054	166.9
<i>H*</i>	1.093, 0.6133, 0.2300, 0.2466, 0.1809, 0.1887, 0.2962, 0.3879, 0.5547, 0.7102, 1.011, 1.412, 1.559, 1.531, 1.053, 0.8326, 0.5409, 0.2550, 0.2480, 0.04181, 0.000	12.98
<i>H[†]</i>	0.1500, 0.0381, 0.05514, 0.07760, 0.07030, 0.1022, 0.1380, 0.1846, 0.3320, 0.5687, 1.174, 1.871, 3.952, 6.146, 6.224, 7.486, 7.032, 4.800, 5.684, 1.284, 0.1222	47.49
<i>H^{†*}</i>	0.5337, 0.09765, 0.07062, 0.1159, 0.1233, 0.1716, 0.1858, 0.3371, 0.5760, 1.123, 1.979, 3.445, 6.230, 7.752, 5.437, 5.182, 3.468, 1.892, 1.575, 0.2776, 0.04508	40.62
<i>R</i>	3389.5, 3571.4, 3573.3, 3758.3, 4680.3, 4354.0, 4218.4, 3880.5, 3523.2, 3454.8, 3334.2, 3102.7, 2732.5, 2116.5, 1141.3, 880.0, 610.8, 327.6, 81.47, 18.18, 2.521	52751.4
<i>D</i>	1.981, 0.4014, 0.3919, 0.5958, 0.5957, 0.8447, 1.015, 1.594, 2.784, 5.136, 9.704, 16.25, 31.42, 43.47, 36.91, 40.70, 34.56, 22.35, 24.81, 5.387, 0.5658	281.5

Impact of I_0 on the total number of tests. In S4 Table and S5 Table we show the total number of tests used and the total number of cases predicted as of June 7, 2021, when only the testing strategy is implemented ($q_0 = 1$), for different values of r_0 and I_0 . As expected, as the I_0 threshold is decreased the number of cases decreases but at the cost of a larger number of tests, especially for large values of r_0 .

S4 Table. Total number of tests.

r_0 ($q_0 = 1$)	$I_0 = 1$	$I_0 = 2072$	$I_0 = 4144$	$I_0 = 8288$
0.02	809857	536180	504002	352928
0.04	1898939	1135992	1044940	681154
0.06	3342937	1791866	1591372	950400
0.08	5208377	2484934	2121557	1158639
0.10	7977256	3342067	2701127	1321335

S5 Table. Total number of cases.

r_0 ($q_0 = 1$)	$I_0 = 1$	$I_0 = 2072$	$I_0 = 4144$	$I_0 = 8288$
0.02	178080	178850	179586	181668
0.04	163608	166244	168707	174310
0.06	148336	155907	161738	171228
0.08	132753	152112	160737	171162
0.10	117361	152129	160845	171308

Acknowledgments

The authors wish to acknowledge the statistical office that provided the underlying data making this research possible: National Institute of Statistics and Censuses, Argentina. LV, IAP, MT, LDV, CEL and LAB acknowledge UNMdP (EXA 956/20), CONICET (PIP 00443/2014) and Ministerio de Ciencia, Tecnología e Innovación, Argentina (BUE 193 - *Programa de articulación y fortalecimiento federal de las capacidades en ciencia y tecnología COVID-19*) for financial support. We also thank the Physics Department of Boston University, for allowing us to use its facilities. Lastly, we thank the anonymous reviewers for their careful reading of our manuscript and their insightful comments and suggestions.

References

1. Ministerio de Salud Argentina, ¿qué medidas está tomando el gobierno?, <https://www.argentina.gob.ar/coronavirus/medidas-gobierno>, (Accessed: 2020-03-24) (March 2020).
2. A. Vespignani, H. Tian, C. Dye, J. Lloyd-Smith, R. Eggo, M. Shrestha, S. Scarpino, B. Gutierrez, M. Kraemer, J. Wu, K. Leung, G. M. Leung, Modelling COVID-19, *Nature Reviews Physics* 2 (2020) 279–281. doi:10.1038/s42254-020-0178-4.
3. E. Javan, S. J. Fox, L. A. Meyers, Estimating the unseen emergence of of COVID-19 in the us, *medRxiv* (2020). doi:10.1101/2020.04.06.20053561.
4. C. Wells, P. Sah, S. Moghadas, A. Pandey, A. Shoukat, Y. Wang, Z. Wang, L. Meyers, B. Singer, A. Galvani, Impact of international travel and border control measures on the global spread of the novel 2019 coronavirus outbreak, *Proceedings of the National Academy of Sciences* 117 (2020) 7504–7509. doi:10.1073/pnas.2002616117.
5. N. Oliver, B. Lepri, H. Sterly, R. Lambiotte, S. Deletaille, M. D. Nadai, E. Letouzé, A. A. Salah, R. Benjamins, C. Cattuto, V. Colizza, N. de Cordes, S. P. Fraiberger, T. Koebe, S. Lehmann, J. Murillo, A. Pentland, P. N. Pham, F. Pivetta, J. Saramäki, S. V. Scarpino, M. Tizzoni, S. Verhulst, P. Vinck, Mobile phone data for informing public health actions across the COVID-19 pandemic life cycle, *Science Advances* 6 (2020). doi:10.1126/sciadv.abc0764.
6. T. Ganyani, C. Kremer, D. Chen, A. Torneri, C. Faes, J. Wallinga, N. Hens, Estimating the generation interval for COVID-19 based on symptom onset data, *Eurosurveillance* 25 (2020) 2000257. doi:10.2807/1560-7917.ES.2020.25.17.2000257.
7. J. Li, P. Yuan, J. Heffernan, T. Zheng, N. Ogden, B. Sander, J. Li, Q. Li, J. Bélair, J. D. Kong, et al., Fangcang shelter hospitals during the COVID-19 epidemic,

- Wuhan, China, Bulletin of the World Health Organization 98 (2020) 830. doi:10.2471/BLT.20.258152.
8. P. Yuan, J. Li, E. Aruffo, Q. Li, T. Zheng, N. Ogden, B. Sander, J. Heffernan, E. Gatov, E. Gournis, S. Collier, Y. Tan, J. Li, J. Arino, J. Bélair, J. Watmough, J. D. Kong, I. Moyles, H. Zhu, Efficacy of “stay-at-home” policy and transmission of COVID-19 in Toronto, Canada: a mathematical modeling study, medRxiv (2020). doi:10.1101/2020.10.19.20181057.
 9. E. Tagliazucchi, P. Balenzuela, M. Travizano, G. Mindlin, P. Mininni, Lessons from being challenged by COVID-19, Chaos, Solitons & Fractals 137 (2020) 109923. doi:10.1016/j.chaos.2020.109923.
 10. M. Amaku, D. T. Covas, F. A. B. Coutinho, R. S. A. Neto, C. Struchiner, A. Wilder-Smith, E. Massad, Modelling the test, trace and quarantine strategy to control the COVID-19 epidemic in the state of São Paulo, Brazil, Infectious Disease Modelling 6 (2021) 46–55. doi:10.1016/j.idm.2020.11.004.
 11. A. Paternina-Caicedo, M. Choisy, C. Garcia-Calavaro, G. España, J. Rojas-Suarez, C. Dueñas, A. Smith, F. De la Hoz-Restrepo, Social interventions can lower COVID-19 deaths in middle-income countries, medRxiv (2020). doi:10.1101/2020.04.16.20063727.
 12. A. Cancino, C. Castillo, P. Gajardo, R. Lecaros, C. Munoz, J. Ortega, H. Ramirez, S. Maria, Report# 3: Estimation of maximal ICU beds demand for COVID-19 outbreak in Santiago (Chile) and the effects of different mitigation strategies, Tech. rep., Technical report (march 2020).
URL <http://covid-19.cmm.uchile.cl>
 13. C. Jiménez Romero, A. Tisnés, S. Linares, Modelo de simulación del COVID-19 basado en agentes. aplicación al caso argentino, Posición (2020).
URL <http://ri.unlu.edu.ar/xmlui/handle/rediunlu/687>
 14. G. Neidhöfer, C. Neidhöfer, The effectiveness of school closures and other pre-lockdown COVID-19 mitigation strategies in Argentina, Italy, and South Korea, ZEW-Centre for European Economic Research Discussion Paper (20-034) (2020). doi:10.2139/ssrn.3649953.
 15. F. Torrente, A. Yoris, D. Low, P. Lopez, P. Bekinshtein, F. Manes, M. Cetkovich, Sooner than you think: A very early affective reaction to the COVID-19 pandemic and quarantine in Argentina, Journal of affective disorders 282 (2021) 495–503. doi:10.1016/j.jad.2020.12.124.

16. S. Figar, V. Pagotto, L. Luna, J. Salto, M. W. Manslau, A. Mistchenko, A. Gamarnik, A. M. G. Saldano, F. Quiros, Community-level SARS-CoV-2 Seroprevalence Survey in urban slum dwellers of Buenos Aires City, Argentina: a participatory research., medRxiv (2020). doi:10.1101/2020.07.14.20153858.
17. H. Ahumada, S. Espina, F. H. Navajas, COVID-19 with uncertain phases: estimation issues with an illustration for Argentina, Available at SSRN 3633500 (2020). doi:10.2139/ssrn.3633500.
18. La Capital, Mar del Plata, en cuarentena: ordenan el cierre de restaurantes, rotiserías, cervecerías y heladerías, <https://www.lacapitalmdp.com/mar-del-plata-en-cuarentena-ordenan-el-cierre-de-restaurantes-rotiserias-cervecerias-y-heladerias/>, (Accessed: 2020-03-17) (March 2020).
19. N. Ferguson, D. Laydon, G. Nedjati-Gilani, N. Imai, K. Ainslie, M. Baguelin, S. Bhatia, A. Boonyasiri, Z. M. Cucunubá, G. Cuomo-Dannenburg, A. Dighe, I. Dorigatti, H. Fu, K. Gaythorpe, W. Green, A. Hamlet, W. Hinsley, L. Okell, S. van Elsland, A. Ghani, Report 9: Impact of non-pharmaceutical interventions (NPIs) to reduce COVID-19 mortality and healthcare demand (March 2020). doi:10.25561/77482.
20. Minnesota Population Center, Integrated public use microdata series, international: Version 7.2 [dataset] (2019). doi:10.18128/D020.V7.2.
21. J. Mossong, N. Hens, M. Jit, P. Beutels, K. Auranen, R. Mikolajczyk, M. Massari, S. Salmaso, G. S. Tomba, J. Wallinga, J. Heijne, M. Sadkowska-Todys, M. Rosinska, W. J. Edmunds, Social Contacts and Mixing Patterns Relevant to the Spread of Infectious Diseases, PLOS Medicine 5 (2008) e74. doi:10.1371/journal.pmed.0050074.
22. L. Fumanelli, M. Ajelli, P. Manfredi, A. Vespignani, S. Merler, Inferring the Structure of Social Contacts from Demographic Data in the Analysis of Infectious Diseases Spread, PLOS Computational Biology 8 (2012) e1002673. doi:10.1371/journal.pcbi.1002673.
23. R. Pastor-Satorras, C. Castellano, P. Van Mieghem, A. Vespignani, Epidemic processes in complex networks, Reviews of Modern Physics 87 (2015) 925–979. doi:10.1103/RevModPhys.87.925.
24. S. M. Moghadas, A. Shoukat, M. C. Fitzpatrick, C. R. Wells, P. Sah, A. Pandey, J. D. Sachs, Z. Wang, L. A. Meyers, B. H. Singer, A. P. Galvani, Projecting hospital utilization during the COVID-19 outbreaks in the United States, Proceedings of the National Academy of Sciences 117 (2020) 9122–9126. doi:10.1073/pnas.2004064117.
25. A. Aleta, D. Martín-Corral, A. Pastore y Piontti, M. Ajelli, M. Litvinova, M. Chinazzi, N. E. Dean, M. E. Halloran, I. M. Longini, S. Merler, A. Pentland, A. Vespignani,

- E. Moro, Y. Moreno, Modeling the impact of social distancing, testing, contact tracing and household quarantine on second-wave scenarios of the COVID-19 epidemic, *medRxiv* (2020). doi:10.1101/2020.05.06.20092841.
26. M. Chinazzi, J. T. Davis, M. Ajelli, C. Gioannini, M. Litvinova, S. Merler, A. Pastore y Piontti, K. Mu, L. Rossi, K. Sun, C. Viboud, X. Xiong, H. Yu, M. E. Halloran, I. M. Longini, A. Vespignani, The effect of travel restrictions on the spread of the 2019 novel coronavirus (COVID-19) outbreak, *Science* 368 (2020) 395–400. doi:10.1126/science.aba9757.
27. D. Duque, D. P. Morton, B. Singh, Z. Du, R. Pasco, L. A. Meyers, COVID-19: How to relax social distancing if you must, *medRxiv* (2020). doi:10.1101/2020.04.29.20085134.
28. D. Meidan, N. Schulmann, R. Cohen, S. Haber, E. Yaniv, R. Sarid, B. Barzel, Alternating quarantine for sustainable epidemic mitigation, *Nature communications* 12 (2021) 1–12. doi:10.1038/s41467-020-20324-8.
29. D. F. Gudbjartsson, A. Helgason, H. Jonsson, O. T. Magnusson, P. Melsted, G. L. Norddahl, J. Saemundsdottir, A. Sigurdsson, P. Sulem, A. B. Agustsdottir, B. Eiriksdottir, R. Fridriksdottir, E. E. Gardarsdottir, G. Georgsson, O. S. Gretarsdottir, K. R. Gudmundsson, T. R. Gunnarsdottir, A. Gylfason, H. Holm, B. O. Jenson, A. Jonasdottir, F. Jonsson, K. S. Josefsdottir, T. Kristjansson, D. N. Magnusdottir, L. le Roux, G. Sigmundsdottir, G. Sveinbjornsson, K. E. Sveinsdottir, M. Sveinsdottir, E. A. Thorarensen, B. Thorbjornsson, A. Löve, G. Masson, I. Jonsdottir, A. D. Möller, T. Gudnason, K. G. Kristinsson, U. Thorsteinsdottir, K. Stefansson, Spread of SARS-CoV-2 in the icelandic population, *New England Journal of Medicine* 382 (2020) 2302–2315. doi:10.1056/NEJMoa2006100.
30. K. Mizumoto, K. Kagaya, A. Zarebski, G. Chowell, Estimating the asymptomatic proportion of coronavirus disease 2019 (COVID-19) cases on board the Diamond Princess cruise ship, Yokohama, Japan, 2020, *Eurosurveillance* 25 (2020) 2000180. doi:10.2807/1560-7917.ES.2020.25.10.2000180.
31. C. Rothe, M. Schunk, P. Sothmann, G. Bretzel, G. Froeschl, C. Wallrauch, T. Zimmer, V. Thiel, C. Janke, W. Guggemos, M. Seilmaier, C. Drost, P. Vollmar, K. Zwirgmaier, S. Zange, R. Wölfel, M. Hoelscher, Transmission of 2019-nCoV infection from an asymptomatic contact in Germany, *New England Journal of Medicine* 382 (2020) 970–971. doi:10.1056/NEJMc2001468.
32. H. Nishiura, T. Kobayashi, T. Miyama, A. Suzuki, S. Jung, K. Hayashi, R. Kinoshita, Y. Yang, A. Yuan, B. and Akhmetzhanov, N. Linton, Estimation of the asymptomatic ratio of novel coronavirus infections (COVID-19), *International Journal of Infectious Diseases* 94 (2020) 154–155. doi:10.1016/j.ijid.2020.03.020.

33. A. Kimball, K. Hatfield, M. Arons, A. James, J. Taylor, K. Spicer, A. Bardossy, L. Oakley, S. Tanwar, Z. Chisty, J. Bell, M. Methner, J. Harney, J. Jacobs, C. Carlson, H. McLaughlin, N. Stone, S. Clark, C. Brostrom-Smith, S. Zane, Asymptomatic and presymptomatic SARS-CoV-2 infections in residents of a long-term care skilled nursing facility — King County, Washington, March 2020, *MMWR. Morbidity and Mortality Weekly Report* 69 (2020) 377–381. doi:10.15585/mmwr.mm6913e1.
34. K. Prem, A. R. Cook, M. Jit, Projecting social contact matrices in 152 countries using contact surveys and demographic data, *PLOS Computational Biology* 13 (2017) e1005697. doi:10.1371/journal.pcbi.1005697.
35. A. Pastore y Piontti, N. Perra, L. Rossi, N. Samay, A. Vespignani, *Charting the next pandemic: modeling infectious disease spreading in the data science age*, Springer, 2018.
36. P. G. Fennell, S. Melnik, J. P. Gleeson, Limitations of discrete-time approaches to continuous-time contagion dynamics, *Physical Review E* 94 (2016) 052125. doi:10.1103/PhysRevE.94.052125.
37. M. Salathé, C. Althaus, R. Neher, S. Stringhini, E. Hodcroft, J. Fellay, M. Zwahlen, G. Senti, M. Battagay, A. Wilder-Smith, I. Eckerle, M. Egger, N. Low, COVID-19 epidemic in Switzerland: on the importance of testing, contact tracing and isolation, *Swiss Medical Weekly* 150 (2020) w20225. doi:10.4414/smw.2020.20225.
38. E. J. Emanuel, G. Persad, R. Upshur, B. Thome, M. Parker, A. Glickman, C. Zhang, C. Boyle, M. Smith, J. P. Phillips, Fair allocation of scarce medical resources in the time of covid-19, *New England Journal of Medicine* 382 (2020) 2049–2055. doi:10.1056/NEJMs2005114.
39. X. Wang, R. Pasco, Z. Du, M. Petty, S. Fox, A. Galvani, M. Pignone, s. C. Johnston, L. Meyers, Impact of social distancing measures on coronavirus disease healthcare demand, central Texas, USA, *Emerging infectious diseases* 26 (2020) 2361–2369. doi:10.3201/eid2610.201702.
40. Quédigital, Un nuevo pedido para conocer cuántas camas de terapia intensiva hay en Mar del Plata, <https://quedigital.com.ar/politica/un-nuevo-pedido-para-conocer-cuantas-camas-de-terapia-intensiva-hay-en-mar-del-plata/>, (Accessed: 2020-10-14) (October 2020).
41. Página12, Mar del plata: crítica situación de las camas de terapia intensiva, <https://www.pagina12.com.ar/288336-mar-del-plata-critica-situacion-de-las-camas-de-terapia-inte>, (Accessed: 2020-08-29) (August 2020).

42. Quédigital, Montenegro: “hoy hay 18 camas libres de terapia, mañana pueden ser 2 y pasado mañana 25”, <https://quedigital.com.ar/politica/montenegro-mahoy-hay-18-camas-libres-de-terapia-en-mar-del-plata-manana-pueden-ser-2-y-pasado-manana-25/>, (Accessed: 2020-10-07) (October 2020).
43. L. Vassallo, I. A. Perez, L. G. Alvarez-Zuzek, J. Amaya, M. F. Torres, L. D. Valdez, C. E. La Rocca, L. A. Braunstein, <https://github.com/SC-MDP/matricesDeContactoMDP> (2021).
44. J. T. Wu, K. Leung, G. M. Leung, Nowcasting and forecasting the potential domestic and international spread of the 2019-nCoV outbreak originating in Wuhan, China: a modelling study, *The Lancet* 395 (2020) 689–697. doi:10.1016/S0140-6736(20)30260-9.
45. Q. Li, X. Guan, P. Wu, X. Wang, L. Zhou, Y. Tong, R. Ren, K. S. Leung, E. H. Lau, J. Y. Wong, et al., Early transmission dynamics in Wuhan, China, of novel coronavirus-infected pneumonia, *New England Journal of Medicine* (2020). doi:10.1056/NEJMoa2001316.
46. J. Riou, C. L. Althaus, Pattern of early human-to-human transmission of Wuhan 2019 novel coronavirus (2019-nCoV), December 2019 to January 2020, *Eurosurveillance* 25 (2020) 2000058. doi:10.2807/1560-7917.ES.2020.25.4.2000058.
47. O. Diekmann, J. Heesterbeek, M. G. Roberts, The construction of next-generation matrices for compartmental epidemic models, *Journal of the Royal Society Interface* 7 (2010) 873–885. doi:10.1098/rsif.2009.0386.
48. C. E. Mills, J. M. Robins, M. Lipsitch, Transmissibility of 1918 pandemic influenza, *Nature* 432 (7019) (2004) 904–906. doi:10.1038/nature03063.
49. A. Jain, K. Nandakumar, A. Ross, Score normalization in multimodal biometric systems, *Pattern recognition* 38 (2005) 2270–2285. doi:10.1016/j.patcog.2005.01.012.
50. Google LLC., Google COVID-19 Community Mobility Reports., <https://www.google.com/covid19/mobility/>, (Accessed: 2020-10-30) (October 2020).
51. M. Ehrhardt, J. Gašper, S. Kilianová, Sir-based mathematical modeling of infectious diseases with vaccination and waning immunity, *Journal of Computational Science* 37 (2019) 101027. doi:10.1016/j.jocs.2019.101027.
52. S. A. Lauer, K. H. Grantz, Q. Bi, F. K. Jones, Q. Zheng, H. R. Meredith, A. S. Azman, N. G. Reich, J. Lessler, The incubation period of coronavirus disease 2019 (COVID-19) from publicly reported confirmed cases: estimation and application, *Annals of internal medicine* 172 (2020) 577–582. doi:10.7326/M20-0504.

53. N. M. Linton, T. Kobayashi, Y. Yang, K. Hayashi, A. R. Akhmetzhanov, S.-m. Jung, B. Yuan, R. Kinoshita, H. Nishiura, Incubation period and other epidemiological characteristics of 2019 novel coronavirus infections with right truncation: a statistical analysis of publicly available case data, *Journal of clinical medicine* 9 (2020) 538. doi:10.3390/jcm9020538.
54. A. W. Byrne, D. McEvoy, A. B. Collins, K. Hunt, M. Casey, A. Barber, F. Butler, J. Griffin, E. A. Lane, C. McAloon, et al., Inferred duration of infectious period of SARS-CoV-2: rapid scoping review and analysis of available evidence for asymptomatic and symptomatic COVID-19 cases, *BMJ open* 10 (2020) e039856. doi:10.1136/bmjopen-2020-039856.
55. Ministerio de Salud Argentina, Covid-19. casos registrados en la república argentina [dataset], <http://datos.salud.gob.ar/dataset/covid-19-casos-registrados-en-la-republica-argentina> (2020).
56. Ministerio de Justicia y Derechos Humanos, Covid-19 - aislamiento y distanciamiento social, <https://www.argentina.gob.ar/justicia/derechofacil/leysimple/covid-19-aislamiento-y-distanciamiento-social>, (Accessed: 2020-09-20) (2020).
57. Z. Hu, C. Song, C. Xu, G. Jin, Y. Chen, X. Xu, H. Ma, W. Chen, Y. Lin, Y. Zheng, et al., Clinical characteristics of 24 asymptomatic infections with covid-19 screened among close contacts in Nanjing, China, *Science China Life Sciences* 63 (2020) 706–711. doi:10.1007/s11427-020-1661-4.
58. Ministerio de Salud de la Ciudad de Buenos Aires, Coronavirus: el ministerio de salud porteño brindó detalles del estudio de seroprevalencia, <https://www.buenosaires.gob.ar/salud/noticias/coronavirus-el-ministerio-de-salud-porteno-seroprevalencia-buenos-aires>, (Accessed: 2020-11-04) (November 2020).